Strain profiles in ion implanted ceramic polycrystals: a new approach based on reciprocal-space crystal selection

H. Palancher, P. Goudeau, Alexandre Boulle, F. Rieutord, V. Favre-Nicolin, Nils Blanc, G. Martin, J. Fouet, Claire Onofri

Strain profiles in ion implanted ceramic polycrystals: a new approach based on reciprocal-space crystal selection

H. Palancher, P. Goudeau, Alexandre Boulle, F. Rieutord, V. Favre-Nicolin, N. Blanc, G. Martin, J. Fouet, C. Onofri

Strain profiles in ion implanted ceramic polycrystals: a new approach based on reciprocal-space crystal selection

H. Palancher*(1), P. Goudeau(2), A. Boulle(3), F. Rieutord(4), V. Favre-Nicolin(5), N. Blanc(6), G. Martin, J. Fouet(1), C. Onofri(1,7)

[1] CEA, DEN, DEC, F-13108 Saint Paul lez Durance, France.

[2] Institut Pprime, CNRS-Université de Poitiers–ENSMA, SP2MI, F-86360 Chasseneuil, France.

[3] Science des Procédés Céramiques et Traitements de Surface (SPCTS), CNRS UMR 7315, Centre Européen de la Céramique, 12 rue Atlantis, 87068 Limoges, France.

[4] CEA, DSM, INAC, F-38054 Grenoble Cedex 9, France.

[5] Université Grenoble-Alpes, F-38041 Grenoble, France, Institut Universitaire de France, F-75005 Paris, France.

[6] Institut NEEL, CNRS-Univ Grenoble Alpes, F-38042 Grenoble, France.

[7] CEMES, CNRS UPR 8011, 29 rue Jeanne Marvig, BP 94347, 31055 Toulouse Cedex 4, France

* *herve.palancher@cea.fr*

Abstract

The determination of the state of strain in implanted materials is a key issue in the study of their mechanical stability. Whereas this question is relatively easily solved in the case of single crystals, it remains a challenging task in the case of polycrystalline materials. In this paper, we take benefit of the intense and parallel beams provided by third generation synchrotron sources combined with a two-dimensional detection system to analyze individual grains in polycrystals, hence obtaining "single crystal – like" data. The feasibility of the approach is demonstrated with implanted UO_2 polycrystals where the in-depth strain profile is extracted for individual grains using numerical simulations of the diffracted signal. The influence of the implantation dose is precisely analyzed for several diffracting planes and grains. It is shown that, at low fluences, the development of strain is mainly

due to ballistic effects with little or no effect from He ions, independently from the crystallographic orientation. At higher fluences, the evolution of the strain profiles suggests a partial and anisotropic plastic relaxation. With the present approach, robust and reliable structural information can be obtained, even from complex polycrystalline ceramic materials.

Main Part

Ion implantation has found many applications in material science encompassing for example the optimization of the mechanical properties of steel[1], doping[2] or spatial organization of nano-objects[3,4] for microelectronics, and the study of nuclear materials under irradiation[5,6]. The alteration of the crystal lattice (i.e. defect creation) due to ion implantation leads to significant strain, which has been extensively studied in the last decades with the view to investigate mainly the mechanical stability of implanted systems (i.e. margins with respect to fracture). In the standard case where grain size is much larger than the implanted thickness[7], it is shown that the component of the strain tensor normal to the sample surface (referred as to ε_{zz} in the following), is the most important one. ε_{zz} is mostly confined in a subsurface layer which thickness depends on the ion energy, and is often heterogeneously distributed along the surface normal.

In the case of single crystals, the strain profile can be determined using dark field electron holography[8] or straightforwardly using high-resolution X-ray diffraction (XRD) on laboratory equipment. In the latter case, the measured high-resolution XRD patterns exhibit strong oscillations in the vicinity of the diffraction peak resulting from the interferences between iso-strain regions from which the phase of the diffracted amplitude (hence the strain profile) can be retrieved[9,10,11,12,13,14].

For polycrystals, powder diffraction with focused X-ray beam is widely used to collect the diffraction pattern. While such an approach, combined with a structural refinement analysis based, for instance, on the Rietveld method[15,16], is efficient for retrieving averaged quantities (average strain, root-mean-squared strain for instance) it is absolutely inefficient to determine the spatial variations of these quantities, although the knowledge of the spatial gradients is essential for the understanding of underlying physical mechanism responsible for structural modifications in implanted materials.

In this paper, we demonstrate that the in-depth strain distribution $\varepsilon_{zz}(z)$ can be accurately determined in individual grains of a polycrystal using synchrotron radiation based XRD coupled with numerical simulations. The potential of this approach is illustrated with He implantations in uranium dioxide (UO_2) polycrystals. This system has been widely investigated within the framework of spent nuclear fuel storage in dry conditions[17,18,19].

Under such conditions, He is produced as a result of the α-decay of radionuclides created during in-reactor irradiation.

The UO_2 polycrystals considered for this study are disks of 8 mm in diameter and about 1 mm thick. They exhibit a 9 µm grain mean size and do not show any preferred crystallographic orientation[7, 20]. A virgin sample has been kept as a reference and three others have been implanted with 60 keV $^4He^+$ ions with fluencies ranging from 1 up to 6×10^{16} ions/cm². This corresponds to damages from 0.4 up to 2.3 displacements per atoms (dpa) as determined using the SRIM Monte-Carlo simulation with 40 and 20 eV displacement energies for U and O atoms respectively[21]. The thickness of the implanted layer is about 0.23 microns. For fluences up to 2×10^{16} ions/cm², strains in the implanted layer have been extensively characterized and a mechanical model has been validated using Laue micro-diffraction measurements[7,22].

XRD patterns were collected on the BM02/D2AM diffraction beamline at the ESRF (Grenoble, France) with a 8.3 keV monochromatic and 1×0.3 mm² (horizontal×vertical) quasi parallel incoming X-ray beam (divergence was 9 and 5 mrad in the horizontal and vertical directions respectively)[23]. Diffraction data were recorded using a XPAD3 2D detector (560×120 pixels with a 130 µm pixel size)[24], mounted on the delta arm of the kappa diffractometer 1 m away from the sample.

This experimental set-up offers the possibility to isolate the Bragg spots coming from individual grains (see Figure 1(a)), the angular resolution of the set-up being much higher than the misorientation between grains. This approach has been applied to our implanted samples around four different UO_2 Bragg reflections (i.e. (220), (311), (222) and (400) covering the elastic anisotropy range). For each reflection, the sample is rocked through the Bragg's law setting over a range wide enough to include all the scattering from the implanted layer. With the 2D detector used in this work, a complete 3D reciprocal space map (RSM) is obtained in a few minutes only, potentially containing the diffraction from several *well separated* grains (see Figure 1(b)). 1D intensity profiles normal to the surface are obtained for several grains by extracting the intensity along a one pixel wide line parallel to the out-of-plane component of the scattering vector (Q_z). These 1D patterns have been then simulated to determine strain profiles using a procedure initially developed for ion implanted single crystals. Briefly, this methodology is based on the dynamical theory, uses B-spline function to model the strain profile and a simulated annealing algorithm as an optimization procedure[13].The comparison between the measured and simulated 1D patterns is given by Figure **2** for a (220)-oriented grain and increasing fluence. It can readily be observed that the agreement between the model and the data is close to perfect over the whole intensity dynamic range. The corresponding strain profiles are displayed in the inset. For each Bragg reflection we analyzed 4-6 different

grains in order to check the reliability of the retrieved strain profiles. The ε_{zz} strain profiles (for grains oriented along (220), (222) and (400)) are shown in Figure 3(a). For each crystallographic orientation, the maximum deviation observed over all grains analyzed (represented as error bars in Figure 3(b)) turns out to be limited. It can hence be concluded that the other characteristics of a given grain (size, thickness[25]) do not significantly influence the ε_{zz} strain profile.

Comparing strain profiles measured on grain with different orientations, it can firstly be mentioned that they all follow the same general trend: sharp increase in the first 0.05 µm (below the sample surface) up to plateau that is observed up to about 0.27 µm then a decrease of ε_{zz} down to zero at about 0.45 µm. For depth higher than 0.45 µm, ε_{zz} is systematically zero. Secondly, however, the values of strains in the [0.05-0.27 µm] depth range strongly depend on grain orientation. This is consistent with previous XRD measurements[20,22] on these samples. This behavior can be rationalized by considering the linear free swelling instead of the ε_{zz} strain[22]. The free swelling corresponds to the isotropic swelling induced by the implantation without any mechanical reaction from the non-implanted substrate, which can be calculated on the basis of the elastic constant of the material. The free swelling profiles are compared in Figure 3(b). An excellent quantitative agreement can be seen, within the experimental error bars, which proves that the swelling is independent of the crystallographic orientation. Finally these profiles are compared with the calculated damage and He concentration profiles. Conclusions are two-fold. Firstly this suggests that the swelling is not caused in this case by the presence of implanted hexogen ion (contrary to Si implanted with H^+ ions[26,27] for instance), this maximum of the He concentration profile being shifted by about 0.05 µm deeper in the UO_2 implanted matrix with respect to the free swelling profile. Secondly the similarity between the damage profile and the free swelling profile (namely for depth in the [0.2; 0.4 µm] range) suggests that the latter mainly originates from ballistic effects, since only this energy loss mechanism is taken into account in the damage profile calculation. Moreover a contribution to the swelling of the electronic energy loss mechanism in the [0; 0.2 µm] depth range can not be excluded.

We now consider the materials implanted at higher fluencies i.e. 4 and 6×10^{16} He ions/cm² (i.e. 1.2 and 2.3 dpa respectively). Conventional powder diffraction evidenced a dramatic decrease of the intensity diffracted by the implanted layer[28], which prevented any accurate strain analysis. Debelle *et al*. observed a similar behavior using HR-XRD on a (100) UO_2 single crystal implanted in very close conditions and concluded to a plastic relaxation[19] with no residual elastic strain. On the contrary, in the case of UO_2 pellets doped with short lived α-emitter (^{238}Pu), Wiss *et al*. suggested that the linear free swelling increases with damage up to a saturation (at 2.5 dpa),

i.e. no relaxation was found[29]. This discrepancy is even more puzzling considering that all three studies provide very similar variations of free swelling with damage for lower damage values (below 0.8 dpa)[22]. Using the same experimental approach, ε_{zz} strain profiles were determined for the four orientations ((220), (311), (222) and (400)). Figure **2** shows the evolution of (220) reflection for increasing fluence. Their comparison confirms our previous laboratory characterizations i.e. a strong decrease of the diffracted intensity especially for the highest strained part of the implanted layer which corresponds to the lowest 2θ values. However in these synchrotron characterizations, because of the much higher signal to noise ratio, oscillations are clearly observed (see Figure 2). Three main conclusions can be derived from this figure. Firstly with increasing implantation fluence, ε_{zz} keeps on increasing to reach locally very high values of 1.86 and 3.15% (for 4 and 6×10^{16} He ions/cm² final implantation dose respectively). The maximal strain values are observed at a depth of about 0.2 µm which also corresponds to the maximum of the calculated damage profile. Moreover it seems that the increase in ion implantation dose mainly affects this depth (located at 0.2 µm below the surface) and not the full implanted layer: the strain levels in the other parts of the implanted layer are less affected. Secondly it must be mentioned that the thickness of the implanted layer does not significantly vary with ion implantation dose: ε_{zz} remains zero for depth higher than 0.45 µm. This room temperature behavior seems to be specific to UO_2 or at least different from what has been observed in ion implanted zirconia for example[30]. Finally, it can be shown that the elastic mechanical model developed for low ion implantation dose (below 0.8 dpa) is not valid for these higher ion implantation doses: it turns out that the free swelling profile do not superimpose for the different crystallographic orientation probed (see Figure 4). In particular, pseudo-free swelling values measured in the (222) oriented grains, are systematically significantly higher than the one measured for (400) and (220) grains. Moreover such an anisotropic strain could explain the embrittlement observed in aged self –irradiated $^{238}PuO_2$ pellet, in which incompatible grain deformation could have occurred[31].

To sum-up on the mechanical behavior of He implanted UO_2 polycrystals at high doses (higher than 0.8 dpa), this work contradicts the hypothesis of a full plastic relaxation[19]: high local elastic strains are found to remain (together with a strong increase of structural disorder, data not shown here) at high fluences. Moreover it is also found that a free swelling cannot be deduced anymore for ion implantation experiments in single or polycrystals which makes impossible any discussion regarding the saturation of free swelling measured in UO_2 pellets doped with ^{238}Pu[29].

To conclude on this work, a very promising methodology has been proposed to characterize out-of-plane strains in ion implanted ceramic polycrystal with an excellent accuracy. The intense and parallel beam of

synchrotron radiation permits the analysis of single grains, hence providing the same type of information as studies conventionally performed on single crystals. This approach has been validated on UO_2 polycrystal implanted with He ion up to an intermediate ion dose (0.4 dpa) and has enabled an accurate definition of strain profiles at higher doses (1.2 and 2.3 dpa), which was not possible using standard analyses.

This methodology should find a wide range of applications: it shows that strain profile analysis does not require systematic use of single crystals. This is all the more interesting that ceramic single crystals often exhibit a mosaïcity .i.e. they are made a large domains with a slight (below 1°) misorientation. If the interest of the work is demonstrated by the analysis of 1D XRD patterns, the analysis of the full reciprocal space scattering (2D [32] an ultimately 3D) should be very helpful for determining the size of extended defects in polycrystals implanted in severe conditions (high energy ions[33] and/or high damage values[34]). Finally this work can be considered as first step towards the use of coherent X-ray diffraction to characterize strains in ion implanted polycrystals[35].

Acknowledgements

Authors are grateful to Nathalie Boudet (Institut Néel, Grenoble) and Jean-Sébastien Micha (CEA, Grenoble) for their help during experiments performed on BM2 and BM32 at the ESRF and to the French CRG and ESRF committees for beamtime provision (MA-2069 and 02-02-822).

Figure Legends

Figure 1: High resolution XRD data collected on a single grain of UO_2 polycrystal implanted with 10^{16} He/cm². (a) Schematic representation of the experiment set-up. (b) 3D reciprocal space maps of 8 different Bragg reflections measured on 8 different (400) grains within a single data collection.

Figure 2: Measured and calculated high resolution XRD study of a single (220) grain within three UO_2 polycrystals implanted with 1, 4 and 6×10^{16} He/cm² respectively. The inset shows the associated profiles of ε_{zz} out-of-plane strain.

Figure 3: Influence of grain orientation on the profiles of both strains (a) and free swelling (b).

Figure 4: "Pseudo" linear free swelling variations with grain orientation at high implantation dose (i.e. 4 and 6×10^{16} He/cm²) for a UO_2 polycrystal. The word "pseudo" is used to underline the impossibility to obtain a single free swelling value relevant for all grain orientations inside a given UO_2 polycrystal implanted at such high doses.

182 **References**

[1] J. Stinville, J. Cormier, C. Templier, and P. Villechaise, "Monotonic mechanical properties of plasma nitrided 316L polycrystalline austenitic stainless steel: Mechanical behaviour of the nitrided layer and impact of nitriding residual stresses", Materials Science and Engineering: A, **605**, 51 – 58 (2014).

[2] A. H. Agajanian, (1981). Ion Implantation in Microelectronics: a Comprehensive Bibliograph. New York: IFI/Plenum.

[3] S. Reboh, M.F. Beaufort, J.F. Barbot, J. Grilhé, and P.F.P. Fichtner, "Orientation of H platelets under local stress in Si" Appl. Phys. Lett. **93**, 022106 (2008).

[4] B. Aspar, M. Bruel, H. Moriceau, C. Maleville, T. Poumeyrol, and A.M. Papon, "Basic mechanisms involved in the Smart-Cut process", Microelectronic Engineering **36**, 233–240 (1997).

[5] S. Moll, T. Jourdan, and H. Lefaix-Jeuland," Direct Observation of Interstitial Dislocation Loop Coarsening in α-Iron" Phys. Rev. Lett **111**, 015503 (2013).

[6] P. Garcia, G. Martin, C. Sabathier, G. Carlot, A. Michel, P. Martin, B. Dorado, M. Freyss, M. Bertolus, R. Skorek, *et al*., "Nucleation and growth of intragranular defect and insoluble atom clusters in nuclear oxide fuels", NIM **B77**, 98-108 (2012).

[7] A. Richard, H. Palancher, E. Castelier, J.-S. Micha, M. Gamaleri, G. Carlot, H. Rouquette, P. Goudeau, G. Martin, F. Rieutord *et al*., "Strains in light-ion-implanted polycrystals: influence of grain orientation », J. App. Cryst. **45,** 826-833 (2012).

[8] N. Cherkashin, S. Reboh, A. Lubk, M.J. Hytch, and A. Claverie, "Strain in Hydrogen-Implanted Si Investigated Using Dark-Field Electron Holography", Appl. Phys. Exp. **6**, 091301 (2013).

[9] S. Leclerc, A. Declémy, M. F. Beaufort, C. Tromas, and J. F. Barbot, "Swelling of SiC under helium implantation", J. Appl. Phys. **98**, 113506 (2005).

[10] N. Sousbie, L. Capello, J. Eymery, F. Rieutord and C. Lagahe, "X-ray scattering study of hydrogen implantation in silicon", J. Appl. Phys. **99**, 103509 (2006).

[11] Y. Zhang, A. Debelle, A. Boulle, P. Kluth, F. Tuomisto, "Advanced techniques for characterization of ion beam modified materials", Current Opinion in Solid State and Materials Science 19, 19–28 (2015).

[12] S. Stepanov and R. Forrest, "Fitting dynamical X-ray diffraction data over the World Wide Web", J. Appl. Cryst. **41**, 958–962 (2008).

[13] A. Boulle, A. Debelle, "Strain-profile determination in ion-implanted single crystals using generalized simulated annealing", J. Appl. Cryst. **43**, 1046-1052 (2010).

[14] S. G. Podorov, N. N. Faleev, K. M. Pavlov, D. M. Paganin, S. A. Stepanov and E. Förster," A new approach to wide-angle dynamical X-ray diffraction by deformed crystals" J. Appl. Cryst. **39**, 652-655 (2006).

[15] P. Scardi and M. Leoni, "Whole powder pattern modelling", Acta Cryst. **A58**, 190-200 (2002).

[16] D. Simeone, G. Baldinozzi, D. Gosset, G. Zalczer and J-F Bérar, "Rietveld refinements performed on mesoporous ceria layers at grazing incidence", J. Appl. Cryst. **44**, 1205–1210 (2011).

[17] W.J. Weber,"Ingrowth of lattice-defects in alpha irradiated UO_2 single-crystals", J. Nucl. Mater. **98**, 206-215 (1981).

[18] P. Garcia, G. Martin, P. Desgardin, G. Carlot, T. Sauvage, C. Sabathier, E. Castellier, H. Khodja, M.-F. Barthe, "A study of helium mobility in polycrystalline uranium dioxide", J. Nucl. Mater. **430**, 156-165 (2012).

[19] A. Debelle, A. Boulle, F. Garrido, L. Thome, "Strain and stress build-up in He-implanted UO2 single crystals: an X-ray diffraction study", J. Mater. Sci. **46**, 4683-4689 (2011).

[20] E. Pizzi, P. Garcia, G. Carlot, H. Palancher, S. Maillard, B. Pasquet, I. Roure, C. Pozo, and C. Maurice, "Iodine Volume Diffusion Measurements in Uranium Dioxide", Defect and Diffusion Forum **323-325**, 197-202 (2012).

[21] J. F. Ziegler, J. P. Biersack and M. D. Ziegler (1985). SRIM – The Stopping and Range of Ions in Matter, http://www.srim.org.

[22] A. Richard, E. Castelier, H. Palancher, J. S. Micha, H. Rouquette, A. Ambard, Ph. Garcia, and Ph. Goudeau, "Multi-scale X-ray diffraction study of strains induced by He implantation in UO2 polycrystals", NIM B **326**, 251-255 (2014).

[23] J.-L. Ferrer, J.-P. Simon, J.-F. Bérar, B. Caillot, E. Fanchon, O. Kaïkati, S. Arnaud, M. Guidotti, M. Pirocchi, and M. Roth, "D2AM, a Beamline with a High-Intensity Point-Focusing Fixed-Exit Monochromator for Multiwavelength Anomalous Diffraction Experiments", J. Synchrotron Rad. **5** 1346-1356 (1998).

[24] K. Medjoubi, T. Bucaille, S. Hustache, J.-F. Bérar, N. Boudet, J.-C. Clemens, P. Delpierre and B. Dinkespiler,"Detective quantum efficiency, modulation transfer function and energy resolution comparison between CdTe and silicon sensors bump-bonded to XPAD3S", J. Synchrotron Rad. **17**, 486-495 (2010).

[25] M. Ibrahim, E. Castelier, H. Palancher, M. Bornert, S. Carré, and J.-S. Micha, "Laue pattern analysis for two-dimensional strain mapping in light-ion-implanted polycrystals", J. App. Cryst. **48**, 1-10 (2015).

[26] S. Reboh, F. Rieutord, L. Vignoud, F. Mazen, N. Cherkashin, M. Zussy, D. Landru, and C. Deguet, "Effect of H-implantation in the local elastic properties of silicon crystals", Applied Physics Letters **103**, 181911 (2013).

[27] N. Cherkashin, F.X. Darras, P. Pochet, S. Reboh, N. Ratel and A. Claverie,"Modelling of point defect complex formation and its application to H+ ion implanted silicon", Acta. Mater. **99**, 187-195 (2015).

[28] A. Richard, Ph.D. Thesis, Poitiers University (France).

[29] T. Wiss, J-P. Hiernaut, D. Roudil, J.-Y. Colle, E. Maugeri, Z. Talip, A. Janssen, V. Rondinella, R.J.M. Konings, H-J. Matzke, *et al*.," Evolution of spent nuclear fuel in dry storage conditions for millennia and beyond", J. Nucl. Mater. **451**, 198–206 (2014).

[30]A. Debelle, J. Channagiri, L. Thome, B. Decamps, A. Boulle, S. Moll, F. Garrido, M. Behar, and J. Jagielski, "Comprehensive study of the effect of the irradiation temperature on the behavior of cubic zirconia", J. Appl. Phys. **115**, 183504 (2014).

[31] C. Ronchi, J.P. Hiernaut, « Helium diffusion in uranium and plutonium oxides », J. Nucl. Mater. **325**, 1–12 (2004).

[32] J. Channagiri, A. Boulle and A. Debelle, "Diffuse X-ray scattering from ion-irradiated materials: a parallel-computing approach", J. Appl. Cryst. **48**, 252–261 (2015).

[33] H. Palancher , R. Kachnaoui, A. Richard, J-C. Richaud, C. Onofri, A. Boulle, H. Rouquette, G. Martin, C. Sabathier, R. Belin, *et al*. "Strain relaxation in He implanted UO_2 polycrystals under thermal treatment: an in-situ XRD study", J. Nucl. Mater. (2015) *submitted*.

[34] C. Onofri, C. Sabathier, H. Palancher, G. Carlot, S. Miro, Y. Serruys, L. Desgranges, M. Legros, "Evolution of extended defects in polycrystalline UO2 under heavy ion irradiation: combined TEM, XRD and Raman study", NIM B 10.1016/j.nimb.2015.08.091, (2015).

[35] N. Vaxelaire , S. Labat, T.W. Cornelius, C. Kirchlechner, J. Keckes, T. Schulli, and O. Thomas, "New insights into single-grain mechanical behavior from temperature-dependent 3-D coherent X-ray diffraction", Acta Mater. **78**, 46-55 (2014).

(a)

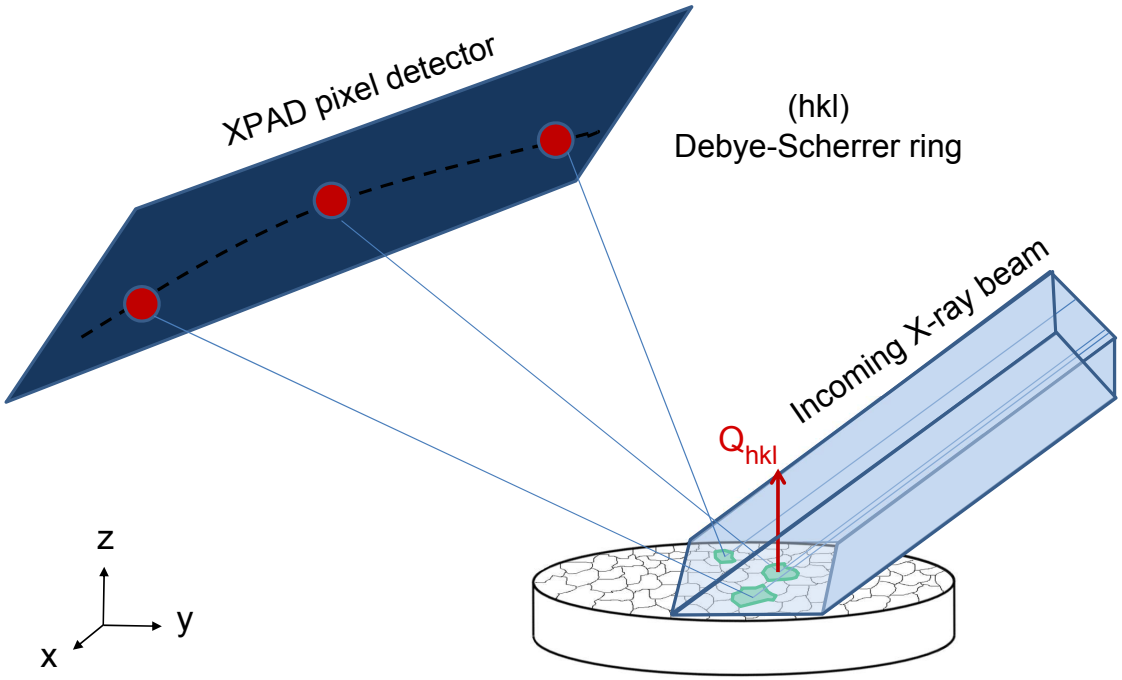
XPAD pixel detector
(hkl)
Debye-Scherrer ring
Incoming X-ray beam
Q_{hkl}
z
y
x

(b)

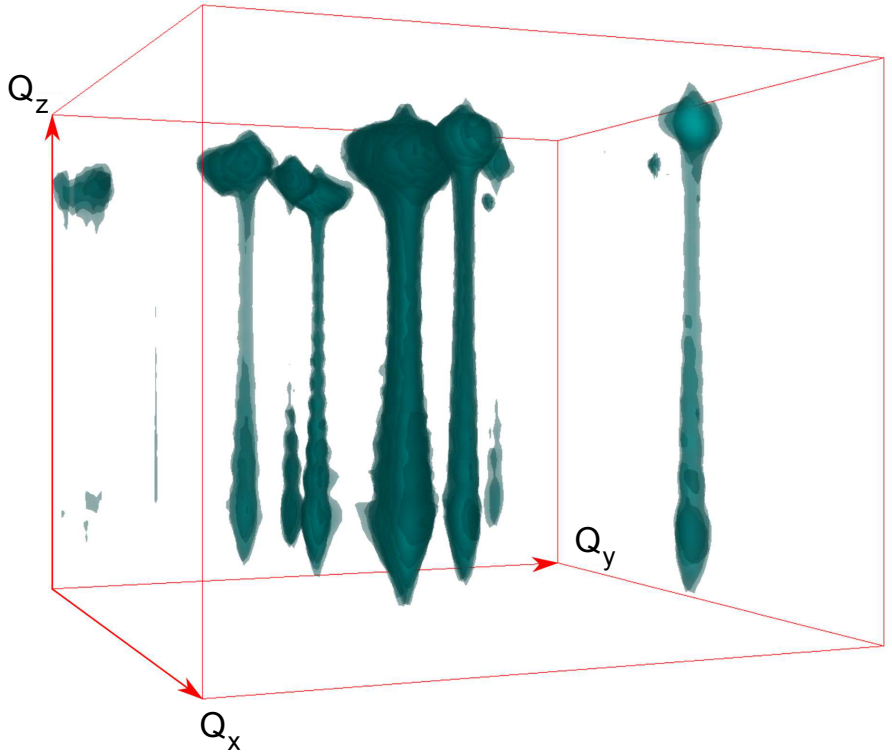
Q_z
Q_y
Q_x

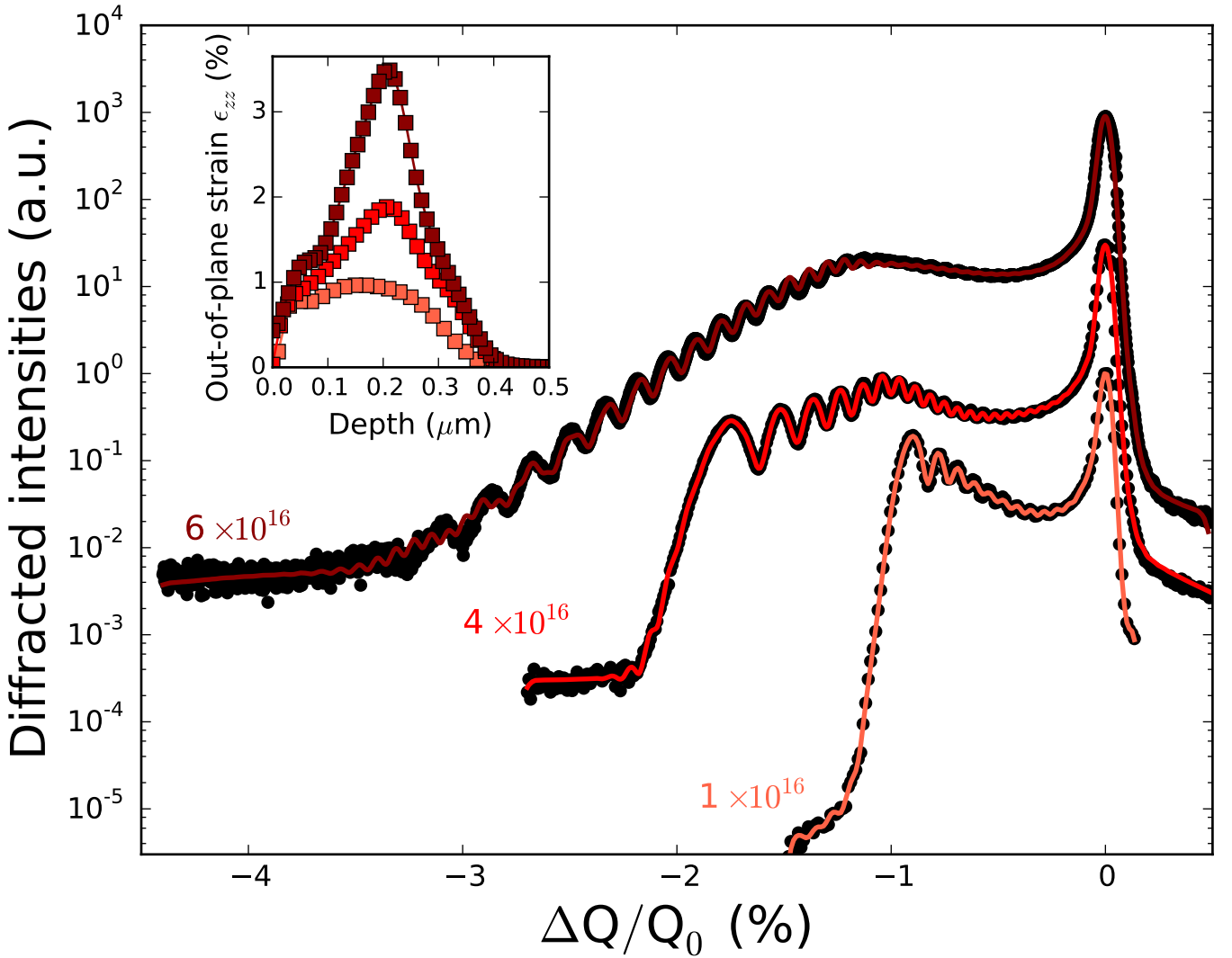
Diffracted intensities (a.u.)
10^4
10^3
10^2
10^1
10^0
10^{-1}
10^{-2}
10^{-3}
10^{-4}
10^{-5}
−4
−3
−2
−1
0
$\Delta Q/Q_0$ (%)
6 $\times 10^{16}$
4 $\times 10^{16}$
1 $\times 10^{16}$
Out-of-plane strain ϵ_{zz} (%)
0
1
2
3
0.0
0.1
0.2
0.3
0.4
0.5
Depth (μm)

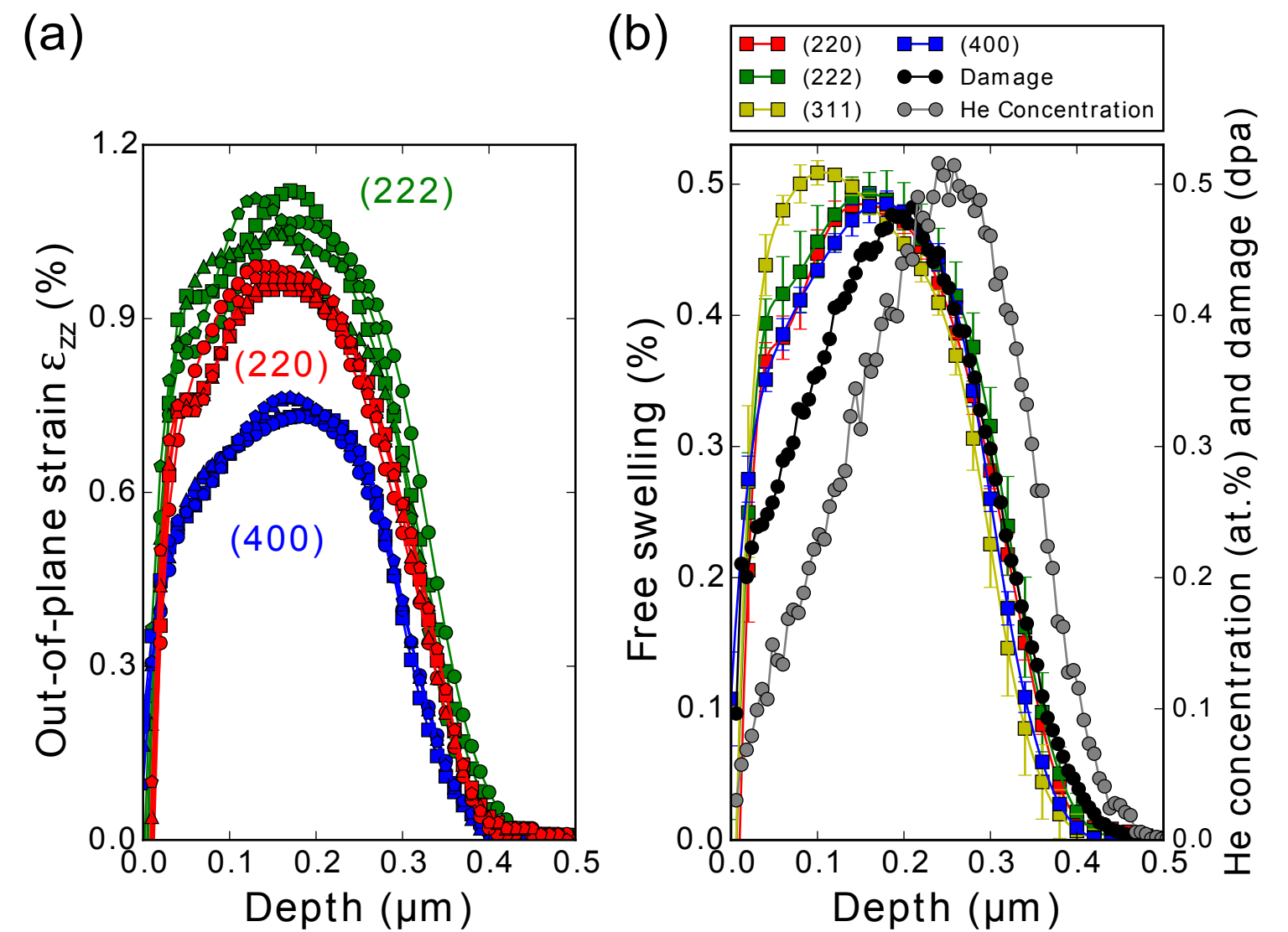
(a)
(b)
(222)
(220)
(400)
Out-of-plane strain ε_{zz} (%)
Depth (μm)
(220)
(400)
(222)
(311)
Damage
He Concentration
Free swelling (%)
He concentration (at.%) and damage (dpa)
Depth (μm)

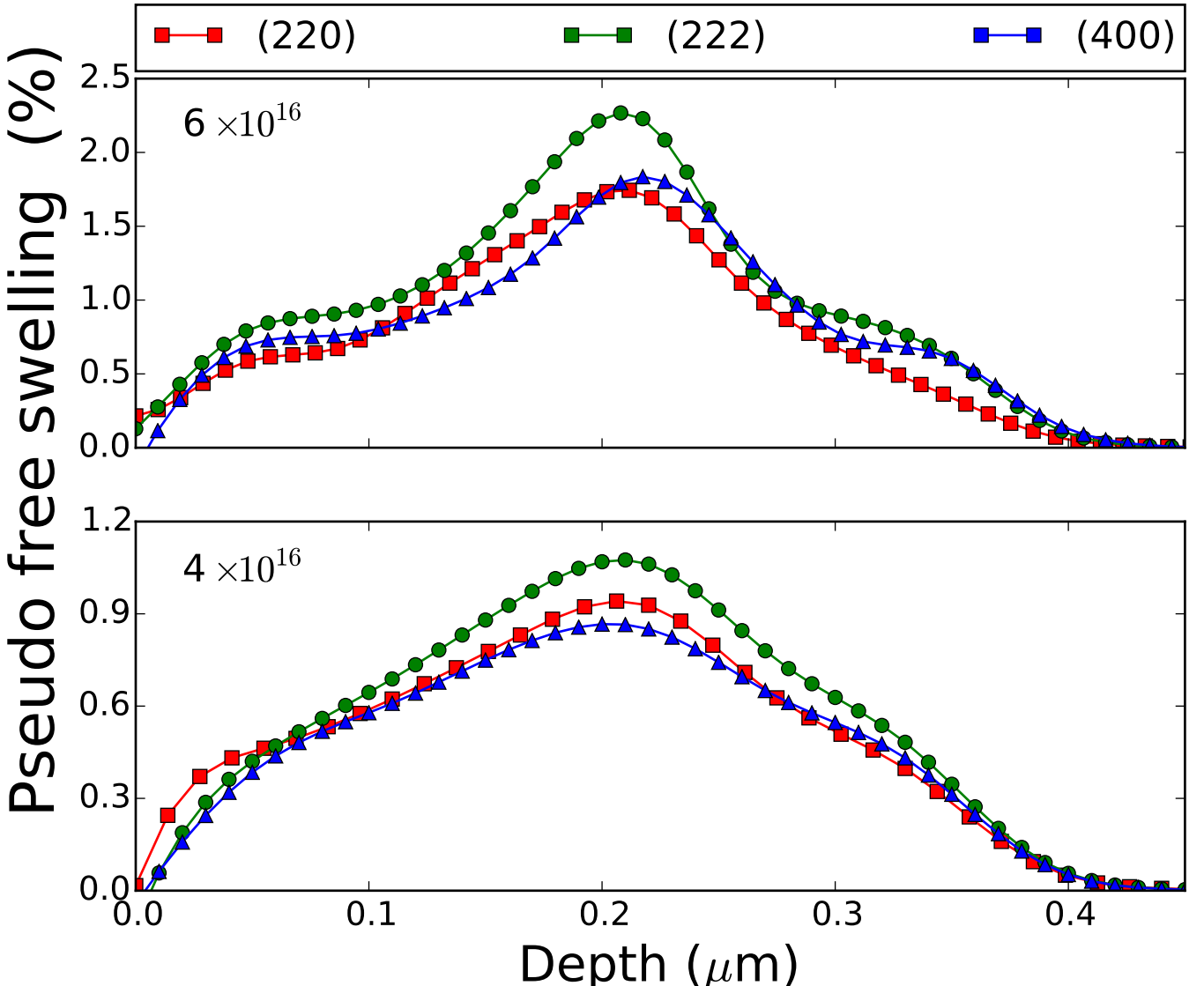
(220)
(222)
(400)
6 ×10^16
4 ×10^16
Pseudo free swelling (%)
Depth (μm)
0.0
0.5
1.0
1.5
2.0
2.5
0.3
0.6
0.9
1.2
0.1
0.2
0.3
0.4